Eur. Phys. J. A **15**, 361–374 (2002)
DOI 10.1140/epja/i2001-10213-1

THE EUROPEAN PHYSICAL JOURNAL A

Shrinking $\hbar$ as a recipe for revealing classical-like properties of optical-potential cross-sections

R. Anni[a]

Dipartimento di Fisica, Università di Lecce and Istituto Nazionale di Fisica Nucleare, Sezione di Lecce, I-73100 Lecce, Italy

Received: 4 September 2001 / Revised version: 25 February 2002 /
Published online: 26 November 2002 –
Communicated by V. Vento

Abstract. A simple recipe for revealing classical-like properties of optical-potential cross-sections is proposed. The recipe is based on the fact that the classical properties are not expected to depend on the actual value of $\hbar$. This allows us to identify the classical-like characteristics of an optical-potential cross-section by simply repeating the calculation with different values of $\hbar$, and observing which properties of the cross-section are invariant. The method is applied to the cross-sections of a few optical potentials used to describe the recent data of light heavy-ion elastic scattering. An improved near-side/far-side decomposition is used to separate the near-side and far-side components of the optical-potential cross-sections.

PACS. 24.10.Ht Optical and diffraction models – 25.70.Bc Elastic and quasielastic scattering – 03.65.Sq Semiclassical theories and applications

1 Introduction

Deep real parts and shallow imaginary ones characterise the optical potentials used to reproduce the recent detailed measurement of the elastic cross-sections of light heavy-ions [1–6]. The cross-sections $\sigma(\theta)$ of these optical potentials show complicated interference patterns making the understanding of the physical phenomena involved in the scattering process difficult. The number of partial waves that contribute to $\sigma(\theta)$ is usually rather large. This allows one to hope that semiclassical methods [7] can be applied for explaining the complicate patterns of the cross-sections in terms of interference between simpler subamplitudes revealing, if possible, simple semiclassical properties of the cross-sections.

The asymptotic limit for $\hbar \to 0$, that will be named the *classical-like* limit, of quantum scattering by a real potential has been well understood for more than fourty years [8]. Usually, this limit is found with the use of asymptotic approximations for the scattering function $S(\lambda)$ ($\lambda = l + \frac{1}{2}$, where l is the angular-momentum quantum number), for the Legendre polynomials $P_l(\cos\theta)$, and for the partial-wave expansion of the scattering amplitude $f(\theta)$. As a result one obtains that the classical-like limit $f_{\rm c}(\theta)$ of $f(\theta)$ can be expressed in terms of one, or more, stationary-phase contributions. The square modulus of the contribution of a stationary-phase point, at $\lambda_i(\theta)$, exactly coincides with the contribution to the classical cross-section at θ from the trajectories with angular momentum λ_i (in units of $\hbar$). Because each stationary-point contribution has also a phase, if more stationary points contribute to $f_{\rm c}(\theta)$ in some angular range, oscillations appear in the classical-like limit $\sigma_{\rm c}(\theta) = |f_{\rm c}(\theta)|^2$ of $\sigma(\theta)$.

A direct comparison of the exact $\sigma(\theta)$ with its asymptotic expression $\sigma_{\rm c}(\theta)$ can provide indications on the possibility of describing the scattering process in terms of classical-like trajectories: trajectories that, as the rays of the geometrical optics, are fixed by a minimum-action principle but have associated phases accounting for the quantum interference phenomenon.

In the scattering process from the optical potentials currently used (also neglecting the complications arising from the presence in the interaction of an imaginary part) the classical integral actions, in units of $\hbar$, are large but, obviously, not infinite. Owing to this, quantum contributions, eventually superimposed to classical-like ones, are usually present in $S(\lambda)$ and in the corresponding $f(\theta)$ and $\sigma(\theta)$. Only in the extreme classical-like limit these quantum contributions are expected to disappear, remaining confined to regions of widths going to zero.

Several methods [7] were developed to extend the semiclassical description to cases in which an imaginary part is present in the potential and the extreme classical-like limit is not well approached. These methods, accounting also for diffraction and reflection above the top of a barrier, considerably extend the possibility of describing semiclassically a scattering process. However, presently, they predict cross-sections in quantitative agreement with the

[a] e-mail: anni@le.infn.it

exact ones only in certain energy ranges, depending on the optical potential considered.

Furthermore, also admitting that we are within the range of validity of some of the available semiclassical methods, their application to practical cases is more difficult than the direct calculation of the exact cross-section. Owing to this, one could ask if some trick exists, which is able to provide quickly some information on the classical-like nature of some properties of $\sigma(\theta)$ using only a standard optical code; without worrying about the complications of the semiclassical techniques, about their ranges of validity, and even without calculating any classical-like quantity.

In this paper one of these possible tricks is investigated. The basic idea is that the classical properties do not depend on $\hbar$. Owing to this, all the properties of a cross-section which do not depend on the value which is attributed to $\hbar$, in the framework of a quantum calculation, can be considered of classical origin.

The main ingredients of this simple recipe, which can be easlily implemented in any standard optical-potential code, are presented in sect. 2. In order to test the method in a simple case, in sect. 3 we present the results obtained for a real optical potential. In sects. 4 and 5 the method is applied to analyze the behavior of two optical-potential cross-sections, fitted to the experimental data of $^{16}\mathrm{O} + ^{12}\mathrm{C}$ at the laboratory energies of 132 and 200 MeV [4].

For the cases considered, the results of the quantum calculation, with the true value of $\hbar$, are first compared with the results of classical calculations. This comparison is not really necessary for the application of the recipe, and is introduced here only to show the reliability of the method to identify correctly classical-like properties.

By varying $\hbar$ the qualitative behavior of the quantum $\sigma(\theta)$ smoothly changes. Considering the oscillations of $\sigma(\theta)$ as arising from the interference between simpler subamplitudes, one observes that, with decreasing $\hbar$, the modulus of some of these subamplitudes continues to modify its behavior (contributing to angular ranges of decreasing width) while that of others becomes insensitive to any further decrease of $\hbar$. The former subamplitudes reveal their quantum origin, the latter their classical-like one.

The comparison of the real $\sigma(\theta)$ (calculated with the true value of $\hbar$) with the fictitious cross-sections (calculated attributing to $\hbar$ values sufficiently small) allows one to obtain easy indications on its classical-like properties.

2 Main ingredients of the recipe

2.1 Classical-mechanics ingredients

Accordingly to classical mechanics, the cross-section for scattering from a potential $V(r)$ is completely determined by the deflection function

$$\Theta(\lambda) = \pi - 2\int_{r_0(\lambda)}^{\infty} \frac{\lambda}{kr^2\sqrt{1 - \frac{V(r)}{E} - \frac{\lambda^2}{k^2r^2}}}\mathrm{d}r, \qquad (1)$$

where $L = \lambda\hbar$ and $p = k\hbar$ are, respectively, the angular and linear momenta, and $r_0(\lambda)$ is the turning point which delimits the classical region of the radial motion from below.

The deflection angle $\Theta(\lambda)$ is the total angle spanned by the vector of the linear momentum along the trajectory with impact parameter $b = \lambda/k$. From its definition $\Theta(\lambda)$ has only an upper limit, it must be lower than π. For attractive potentials the minimum of $\Theta(\lambda)$ can be any negative values, depending on the potential, and can also become $-\infty$ at certain λ values, when the *orbiting*, or *spiral scattering*, phenomenon occurs.

At large distances from the scattering center, the trajectories with a deflection angle between $-2n\pi$ and $(-2n+1)\pi$, with $n = 0, 1, \ldots$, have their initial and final parts in the same half of the scattering plane divided along the line parallel to the initial linear momentum and passing through the origin. These trajectories are usually named *near-side* (N) trajectories. Similarly the trajectories with a deflection angle between $(-2n-1)\pi$ and $-2n\pi$, with $n = 0, 1, \ldots$, have their initial and final parts in opposite halves of the scattering plane. These trajectories are usually named *far-side* (F) trajectories. In both cases the index n counts the number of times the trajectories have encircled the origin.

The angle $\theta(\lambda)$ at which the particles are scattered, and observed, is by definition contained in the interval 0-π, and it is obtained from the deflection angle $\Theta(\lambda)$ using the relation

$$\theta(\lambda) = \arccos[\cos\Theta(\lambda)]. \qquad (2)$$

The relation (2) "physically" corresponds to *folding* the plane (λ, Θ) first up, along the line $\Theta = 0$, and then down, along the line $\Theta = \pi$. The folding must be repeated until all the parts of $\Theta(\lambda)$ fall in the scattering angle range.

An artist's view of this folding procedure is given in fig. 1. The thick line gives $\Theta(\lambda)$ as a function of the impact parameter b. The continuous and dashed parts of this line indicate the branches of $\Theta(\lambda)$ corresponding to N and F trajectories, respectively, and the labels designate the branches of $\Theta(\lambda)$ producing a bijective mapping from b to θ. The dependence of $\theta(\lambda)$ on b, obtained using the folding procedure, is given in the upper panel by the thin lines.

The deflection function shown in fig. 1 has the typical characteristics which are expected for scattering by a nuclear strongly attractive potential with a Coulomb repulsive tail. The interplay between the attractive and repulsive forces produces the appearance of a narrow minimum, a *nuclear* rainbow, and a broad maximum, a *Coulomb* rainbow. The positions of the points corresponding to these rainbows are indicated in the figure with the symbols θ_n and θ_C, respectively.

The i-th branch $\theta_i(\lambda)$ contributes to the classical cross-section, at angles between the minimum and the maximum value of $\theta_i(\lambda)$, with a term

$$\sigma_i(\theta) = \frac{\lambda_i(\theta)}{k^2\sin\theta}\left|\frac{\mathrm{d}\lambda_i(\theta)}{\mathrm{d}\theta}\right|, \qquad (3)$$

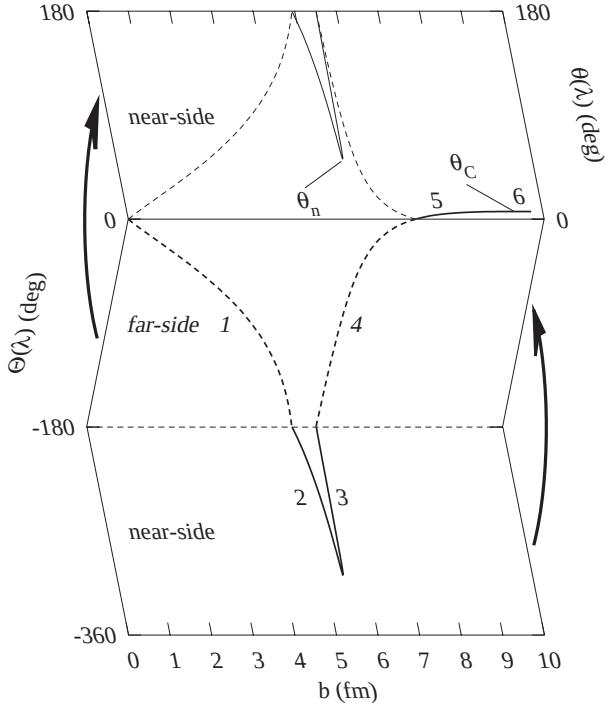

Fig. 1. Artist's view of the folding procedure transforming deflection angles into scattering angles.

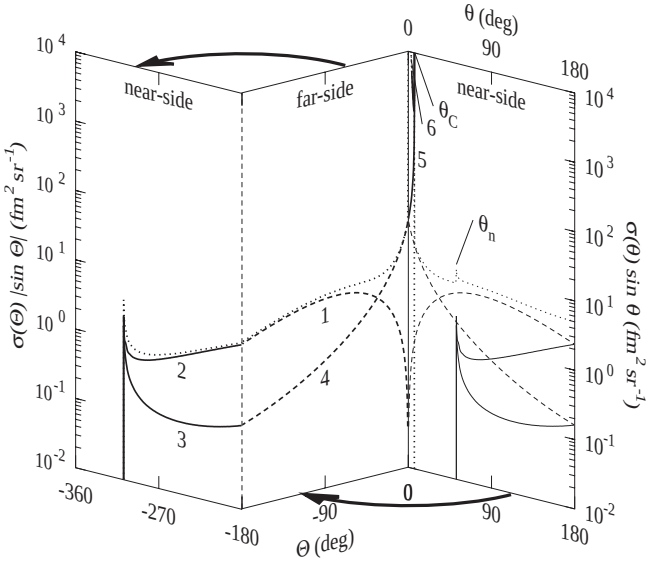

Fig. 2. Artist's view of the cross-section unfolding procedure transforming back the scattering angles into deflection angles.

where $\lambda_i(\theta)$ is the inverse function of $\theta_i(\lambda)$. The full classical cross-section is finally given by

$$\sigma_{\rm C}(\theta) = \sum_j \sigma_j(\theta), \tag{4}$$

where the index j runs over the indices of all the branches of $\theta(\lambda)$ contributing to the scattering angle θ.

As a result, with the exclusion of the few cases in which the deflection functions are particularly simple, the structure of $\sigma_{\rm C}(\theta)$ is rather complicated. Several and different branches of $\Theta(\lambda)$ contribute to $\sigma_{\rm C}(\theta)$ in different angular ranges. For example, to the cross-section of the deflection function shown in fig. 1, the branches 1, 4, 5, and 6 contribute in the range $0 < \theta < \theta_{\rm C}$, the branches 1 and 4 in the range $\theta_{\rm C} < \theta < \theta_{\rm n}$, and finally the branches 1, 2, 3 and 4 in the range $\theta_{\rm C} < \theta < \pi$. The cross-section goes to infinity for θ approaching from the left $\theta_{\rm C}$ and from the right $\theta_{\rm n}$ (rainbow singularities). The cross-sections $\sigma_{4,5}$ and $\sigma_{1\text{-}4}$ are divergent at $\theta = 0$ and $\theta = \pi$, respectively, because of the presence of the term $1/\sin\theta$ in (3) (*glory* singularities).

The resulting complicated behavior of $\sigma_{\rm C}(\theta)$ mainly arises from the folding procedure transforming deflection angles into scattering angle. A simpler representation can be obtained *unfolding* the cross-section, *i.e.* reassigning the contributions $\sigma_i(\theta)$ to the deflection angle range from which they are originated.

An artist's view of this unfolding procedure is shown in fig. 2 for the cross-section corresponding to the deflection function of fig. 1. In this figure the thin and thick lines (solid for N, dashed for F, and dotted for the summed contributions) show the folded and the unfolded contributions, respectively. The labels identify the contributions from the different branches of $\Theta(\lambda)$.

To get rid of the glory singularities we have preferred to plot $\sigma(\theta)\sin\theta$ and $\sigma(\Theta)|\sin\Theta|$ rather than the cross-sections. The unfolded curves have a continuous behavior at $\Theta = -180°$ and the full $\sigma(\Theta)|\sin\Theta|$ is made up using only the contributions of three new branches of the deflection function. The first is made up from the old branches 1 and 2, and corresponds to angular momenta smaller than the nuclear-rainbow one $\lambda_{\rm n}$. The second is made up from the old branches 3, 4, and 5, and corresponds to angular momenta from $\lambda_{\rm n}$ to the angular momentum $\lambda_{\rm C}$ of the Coulomb rainbow. The last is the old branch 6, and corresponds to angular momenta larger than $\lambda_{\rm C}$.

If one limits oneself to separate, in the original scattering angle range, the N from the F contributions, one obtains another representation of the cross-section that in some cases can become as simple as the unfolded representation. The case shown in fig. 2 is one of these cases. Only two branches (1 and 4) contribute to the F cross-section in the whole scattering angle range, and the remaining four branches, in separated pairs, contribute to the N cross-section. The branches 5 and 6 contribute only for $\theta < \theta_{\rm C}$ and the branches 3 and 4 contribute only for $\theta > \theta_{\rm n}$.

2.2 Quantum-mechanics ingredients

Accordingly to quantum mechanics, the cross-section for scattering from a potential $V(r)$ is completely determined by the scattering function $S(\lambda)$. This quantity defines the scattering amplitude

$$f(\theta) = \frac{i}{k}\sum_{l=0}^{\infty}\lambda[1 - S(\lambda)]P_{\lambda-\frac{1}{2}}(\cos\theta), \tag{5}$$

and the cross-section $\sigma(\theta) = |f(\theta)|^2$.

In the limit $\hbar \to 0$ a link appears between $S(\lambda)$ and the classical deflection function $\Theta(\lambda)$. These two quantities are in fact connected by the relation

$$\lim_{\hbar \to 0} \frac{\mathrm{d} \arg S(\lambda)}{\mathrm{d}\lambda} = \Theta(\lambda). \tag{6}$$

Thanks to this link, a classical-like expression for $\sigma(\theta)$ is obtained substituting the Legendre polynomials with the first term of their non-uniform asymptotic expansion, transforming the partial-wave expansion into a sum of integrals, and evaluating asymptotically these integrals using the stationary-phase method (ref. [7] p. 49-63).

The properties of the deflection function fix the number of the stationary-phase points $\lambda_i(\theta)$ which contribute to the asymptotic estimate $f_{\mathrm{c}}(\theta)$ of $f(\theta)$ at the angle θ. Each $\lambda_i(\theta)$ gives to $f_{\mathrm{c}}(\theta)$ a contribution

$$f_i(\theta) = A_i(\theta) \exp[i\alpha_i(\theta)], \tag{7}$$

where $A_i(\theta)$ and $\alpha_i(\theta)$ are, respectively, the modulus and the phase of $f_i(\theta)$.

The dependence of $\lambda_i(\theta)$ on θ is the same predicted by classical mechanics for the corresponding branch of the classical deflection function. Furthermore, the rule fixing the scattering angular ranges to which λ_i contributes is the same which holds in classical mechanics. Owing to this, in analogy to (4), one obtains

$$f_{\mathrm{c}}(\theta) = \sum_j f_j(\theta). \tag{8}$$

Each $A_i^2(\theta)$ is equal to a corresponding classical $\sigma_i(\theta)$, given by (3), and does not depend on $\hbar$. This classical invariance of $A_i(\theta)$ can be used to obtain a signature of the dominance of contributions from the classical-like amplitudes $f_i(\theta)$ in a quantum cross-section by simply observing the changes of this quantity produced by varying $\hbar$.

The analysis is particularly simple if only one branch of the classical $\Theta(\lambda)$ contributes to the cross-section in a certain, or in the whole, scattering angle range. In this case the signature of the dominance of a classical-like contribution is the observation that the quantum $\sigma(\theta)$ does not change by shrinking $\hbar$. The phase associated to the classical-like amplitude is completely unrelevant.

The situation is slightly more complicated in the angular ranges in which two, or more, branches of the classical $\Theta(\lambda)$ contribute to the cross-section. Omitting for simplicity the specification of the different quantities from θ, in these cases two, or more, f_i contribute to the asymptotic estimate f_{c} of f, and the phases α_i produce interference effects in the asymptotic estimate $\sigma_{\mathrm{c}} = |f_{\mathrm{c}}|^2$ of the cross-section.

The phases α_i are essentially, apart from a common renormalization term, the integral action (in units of $\hbar$) accumulated along the classical trajectories with angular momentum λ_i, and the difference between any pair of phases $\alpha_i - \alpha_j$ goes to infinity as $\hbar$ goes to zero. Owing to this, in these situations, even in the limit $\hbar \to 0$ the interference oscillations do not disappear. The oscillation period goes to zero, and σ_{c} continues to oscillate between an upper and a lower value. In this limit the quantum cross-section becomes equal to σ_{c}, and the classical-mechanics result (4) can be obtained only by averaging σ_{c} over the finite resolution of the experimental device used to count the scattered particles.

Even in these more complicated situations a clear indication of the dominance of classical-like contributions can be obtained by repeating the quantum calculation varying $\hbar$. Let us assume, for example, that in a certain angular range, only the contribution from the branches labelled i and j of the classical $\Theta(\lambda)$ are expected. In this case σ_{c} has the form

$$\sigma_{\mathrm{c}} = A_i^2 + A_j^2 + 2A_iA_j \cos(\alpha_i - \alpha_j). \tag{9}$$

The σ_{c} values are included between the upper limit $(A_i + A_j)^2$, corresponding to maximal constructive interference, and the lower limit $(A_i - A_j)^2$, corresponding to maximal destructive interference. These upper and lower limits are the upper and lower envelopes of all the σ_{c} curves calculated by varying $\hbar$. This is due to the fact that the $A_{i,j}$ do not depend on $\hbar$ (they are equal to $\sigma_{i,j}^{1/2}$, where the $\sigma_{i,j}$ are the corresponding classical cross-sections), while $\alpha_i - \alpha_j$ is inversely proportional to $\hbar$. In the following, these envelopes and the delimited region will be named *classical interference limits* and *classical interference region*, respectively, or more briefly *interference limits* and *interference region*.

The quantum $\sigma(\theta)$, if entirely dominated by two classical-like contributions, must be expressible in the form (9), and must have as upper and lower envelopes the classical interference limits. Should we calculate $\sigma(\theta)$ using smaller values of $\hbar$ we would only observe the sliding of $\sigma(\theta)$, with an increasing number of oscillations, in the classical interference region. On the other hand, the fact that the $\sigma(\theta)$ satisfies this property can be considered a signature of the dominance of two classical-like contributions.

The problem remains of finding the classical interference limits. One obvious possibility is represented by calculating the classical cross-sections σ_i. For an arbitrary number of branches, contributing to the cross-section at a given θ, the upper interference limit is given by

$$\sigma_u(\theta) = \left[\sum_i \sigma_i^{1/2}(\theta) \right]^2. \tag{10}$$

The lower interference limit can be calculated by finding at each θ the value M of the index of the largest amongst the $\sigma_i^{1/2}(\theta)$. Indicating with $\delta(\theta)$ the quantity

$$\delta(\theta) = \sigma_M^{1/2}(\theta) - \sum_{i \neq M} \sigma_i^{1/2}(\theta), \tag{11}$$

the lower interference limit is given by

$$\sigma_l(\theta) = \begin{cases} 0 & , \text{for } \delta(\theta) \leq 0\,, \\ \delta^2(\theta) & , \text{for } \delta(\theta) > 0\,. \end{cases} \tag{12}$$

Equations (10) and (12) become

$$\sigma_{u,l}(\theta) = [\sigma_i^{1/2}(\theta) \pm \sigma_j^{1/2}(\theta)]^2 \tag{13}$$

in the angular ranges in which only the two branches i and j contribute to the cross-section.

Without using any classical calculation the interference limits can also be found empirically, using a standard optical-potential code and calculating the quantum cross-sections by attributing to $\hbar$ different values, sufficiently smaller than the physical value and constructing, if observed, the common lower and upper envelopes of the cross-section curves. In the cases that we have analyzed the tendency of the cross-section curves to have these common envelopes was clearly observed by attributing to $\hbar$ values from 3 to 4 times smaller than the true value. It may be that, in different cases, this tendency is not observed using reduced $\hbar$ values belonging to this range. However, even in these cases we can give an answer (negative) to the question of whether the quantum cross-section is dominated by classical-like contributions. If also with the reduced values of $\hbar$ we are far from the region where $\sigma(\theta) \simeq \sigma_c(\theta)$, *a fortiori*, we must be even farther with the real value of $\hbar$.

Using this simple method without any prudence there is, however, the risk to miss the observation of classical-like contributions in situations in which these are actually present. The fact is that the classical-like limit of different scattering mechanisms is reached, by shrinking $\hbar$, with different rapidity. When many scattering mechanisms contribute to the quantum scattering phenomenon it may happens that some of these mechanisms have well approached this limit, while others, of wave origin (like reflection and diffraction in the region of rapid variation of the interaction), continue to contribute significantly to the interference pattern of the full cross-sections calculated with reduced values of $\hbar$.

To limit this possible risk, without being forced to use very small values of $\hbar$, it is convenient to try to separate, in the full quantum amplitude $f(\theta)$ the contributions from the different mechanisms. To this scope we use here an improved near-side/far-side (NF) decomposition of order 1 [9]. The NF decomposition, proposed in its usual formulation by Fuller [10], tries to separate in the full $f(\theta)$ the contributions from the different scattering mechanisms using the same NF separation criterion that can be used to separate the contributions from different trajectories to the classical cross-section. The N and F cross-sections are less structured than the full $\sigma(\theta)$. This will allow us to appreciate, for example, the existence of well-defined upper and lower envelopes in the quantum F cross-sections, calculated with $\hbar$ below a certain value, even when the quantum contributions to the N amplitude prevent the full $\sigma(\theta)$ to have upper and lower envelopes defined.

The improved NF decomposition here used strongly reduces the importance of unphysical contributions appearing in a preliminary proposal of the shrinking $\hbar$ method [11] where the conventional Fuller's NF decomposition [10] was used.

2.3 Role of the imaginary potential and properties of $S(\lambda)$

The above scheme is well suited to bring out classical-like contributions in the cross-section for scattering by a real potential, but it cannot be directly applied to cases in which an imaginary potential is introduced, to simulate the effects of the population of channels different from the elastic one.

The imaginary part $W(r)$ of the potential, if negative, removes flux from the elastic channel and the time dependence of the probability density, $\rho(\mathbf{r},t) = |\psi(\mathbf{r},t)|^2$, of finding the scattering partners at time t at a relative position $\mathbf{r}$ satisfies the equation (ref. [7], pp. 7 and 49)

$$\frac{\partial \rho(\mathbf{r},t)}{\partial t} + \mathrm{div}\mathbf{j}(\mathbf{r},t) = \frac{2W(r)}{\hbar}\rho(\mathbf{r},t), \tag{14}$$

where $\mathbf{j}(\mathbf{r},t)$ is the probability current density. The above equation suggests the interpretation of the quantity $w = -2W(r)/\hbar$ as the transition rate out of the elastic channel.

With this interpretation of w the form of the classical cross-section given by eq. (3) remains the same, apart for the introduction on the r.h.s of a multiplicative factor

$$P(\lambda) = \exp\left(\frac{1}{2\hbar}\int_{r_0(\lambda)}^{\infty} \frac{\frac{W(r)}{E}}{\sqrt{1-\frac{V(r)}{E}-\frac{\lambda^2}{k^2r^2}}}\mathrm{d}r\right), \tag{15}$$

expressing the probability that the particles with angular momentum λ are not removed from the elastic channel during their motion along the classical trajectory. This form of the cross-section is just that obtained using the naive WKB approximation [12] to estimate $S(\lambda)$, the stationary-phase method to evaluate $f(\theta)$, and neglecting the interference effects. In this approximation, the probability that the particles with angular momentum λ are not removed from the elastic channel can be identified with $|S(\lambda)|^2$, which has exactly the dependence (15) from the imaginary part of the potential.

In accordance with this picture, in the search process of the classical interference limits by varying $\hbar$ (in order to keep constant the survival probability factor) the imaginary potential must be scaled with the same factor used for $\hbar$. This will be the additional caution used to look for traces of classical-like contributions in the quantum $\sigma(\theta)$.

Apart from in the cross-section, traces of classical-like contributions can also be found in the behavior of $|S(\lambda)|$ and of $\mathrm{d}\arg S(\lambda)/\mathrm{d}\lambda$. In the following, this last quantity will be named *quantum deflection function* and indicated with $\Theta_Q(\lambda)$.

If the asymptotic classical-like region is well approached both $|S(\lambda)|$ and $\Theta_Q(\lambda)$ are expected not to depend on the value of $\hbar$, if plotted *versus* the impact parameter $b = \lambda/k$.

The conventional optical-potential codes provide the values of $S(\lambda)$ at *half-integer* positive λ values. These values can be used directly to plot $|S(\lambda)|$ *versus* the impact

parameter b, and using the finite difference formula

$$\Theta_{\rm Q}(\lambda) = \frac{{\rm d}\arg S(\lambda)}{{\rm d}\lambda} \simeq \frac{\arg S(\lambda+\Delta\lambda) - \arg S(\lambda-\Delta\lambda)}{2\Delta\lambda}, \tag{16}$$

with $\Delta\lambda = 0.5$, they often also provide a reasonable approximation for $\Theta_{\rm Q}(\lambda)$ at *integer* λ values. In the cases here considered the angle α between two successive $S(\lambda)$ values, plotted in the complex plane, is taken as the convex one. Only as an extreme precaution the quantity $\Theta_{\rm Q}(\lambda)$ was estimated, outside our conventional optical code, using eq. (16) with a step $\Delta\lambda = 0.1$ for $\alpha > \frac{\pi}{4}$ and of 0.5 elsewhere.

The fact that the values of $|S(\lambda)|$ and $\Theta_{\rm Q}(\lambda)$, calculated with different values of $\hbar$ and plotted against b, lie on the same curve can be considered a sign of the relevance of classical-like contributions in the scattering process. However this fact, alone, does not guarantee that $f(\theta)$ is well approximated by $f_{\rm c}(\theta)$ given by (8). The realization of this classical-like limit for $f(\theta)$ also requires that the integrals, in which the partial-wave expansion of $f(\theta)$ is transformed, can be approximated by the stationary-phase method and that, at the stationary-phase points, the Legendre functions are well approximated by the first term of their non-uniform asymptotic expansion.

The stationary-phase method fails in a neighborhood of the classical rainbow angles and the uniform method (ref. [7], p. 58) allows an estimation of $f(\theta)$ in terms of Airy functions. The uniform approximation substitutes the singularity of the classical cross-section, followed by the sharp shadow region, with a maximum in the lit region followed by a decrease of the cross-section in the shadow region. The interference oscillations in the lit region have a period increasing by approaching the maximum. In the limit $\hbar \to 0$ the oscillation period goes to zero rather slowly, while the maximum moves towards the rainbow angle and the cross-section decreases more and more rapidly in the shadow region. Therefore, in general, we can expect a precise identification of the classical interference region only using very small $\hbar$ values.

Similar drawbacks are also expected in the extreme backward direction, where the usual non-uniform approximation for the Legendre functions does not hold (ref. [7], p. 89). This approximation is responsible for the presence of the factor $1/\sin\theta$ in the asymptotic cross-section and, consequently, for the classical glory singularity.

These typical quantum effects are, however, standard, and one can easily account for them, recognizing their presence in the cross-sections calculated with reduced values of $\hbar$.

3 Real optical-potential cross-section

To test the effectiveness of the method based on the variation of $\hbar$, we first consider the cross-section of a fictitious real optical potential having a conventional Woods-Saxon form factor with parameters $V_0 = 282.2$ MeV, $R_v = 2.818$ fm and $d_v = 0.978$ fm. This potential is the real part of one of those used for fitting the elastic-scattering cross-section of ^{16}O + ^{12}C at $E_{\rm lab} = 132$ MeV [4]. For all the cases here considered, the Coulomb part of the interaction is described using an analytical potential that closely approximates [13] the Coulomb potential of two uniformly charged spheres with radii of 3.54 fm and 3.17 fm. We note, in passing, that the classical deflection function and cross-sections shown in the artist's views of subsect. 2.1 (figs. 1 and 2) are those of this potential. In the following, we will refer to the different branches of the deflection function of this potential using the same indices used in the figs. 1 and 2.

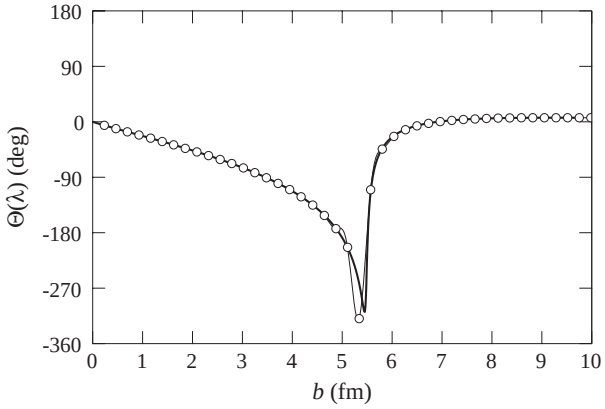

Fig. 3. Classical (thick curve) and quantum (open dots) deflection functions. The thin curve interpolates the dots.

3.1 Comparison with classical quantities

The thick solid line in fig. 3 shows the classical deflection function $\Theta(\lambda)$, as a function of the impact parameter b. This line, as similar ones for the other cases considered, shows the cubic spline interpolation of the $\Theta(\lambda)$ values calculated using eq. (1). The open dots in fig. 3 show the values of $\Theta_{\rm Q}(\lambda)$ estimated by using eq. (16) at integer λ values. The thin curve gives the cubic spline interpolation of the calculated points. The agreement between the dots and the thick curve is impressive and the small differences between the thin and the thick lines may be a consequence of the spline used to interpolate the dots.

The classical deflection function shows a maximum of about 7° at $b_{\rm C} \simeq 9.3$ ($\lambda_{\rm C} \simeq 40.2$) and a minimum of about −310° at $b_{\rm n} \simeq 5.4$ ($\lambda_{\rm n} \simeq 23.5$). The corresponding Coulomb and nuclear rainbows are located at $\theta_{\rm C} \simeq 7°$ and $\theta_{\rm n} \simeq 50°$, respectively. At $b \neq 0$, the deflection function $\Theta(\lambda)$ crosses three times values for which $\sin\theta = 0$. Two glory singularities are expected at $\theta = 180°$ and one, additional to the Coulomb singularity, at $\theta = 0°$.

In panel (a) of fig. 4 the thick curve shows the ratio of the full classical-mechanics cross-section $\sigma_{\rm C}(\theta)$ (4) to the Rutherford one $\sigma_{\rm R}(\theta)$. The thin solid and dashed curves show the contributions $\sigma_i(\theta)$ (3) from the different branches, N and F respectively, of $\Theta(\lambda)$. The labels identify the contributions for $i = 1, 2, 3$, and 4. The appearance of the rainbow singularities is clear, as that of the

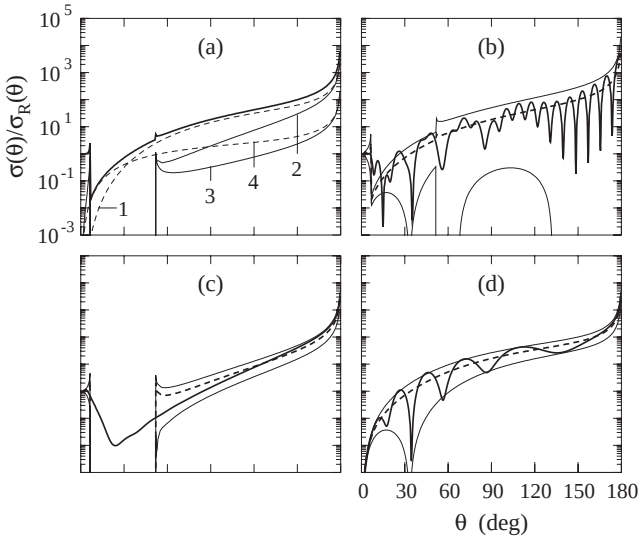

Fig. 4. (a) Classical cross-section (thick line), N (thin solid lines) and F (thin dashed lines) contributions to the classical cross-section; (b) quantum (thick solid line) and classical (thick dashed line) cross-sections , the thin lines show the interference limits; (c) and (d) the same as in panel (b) for the N and F cross-sections, respectively.

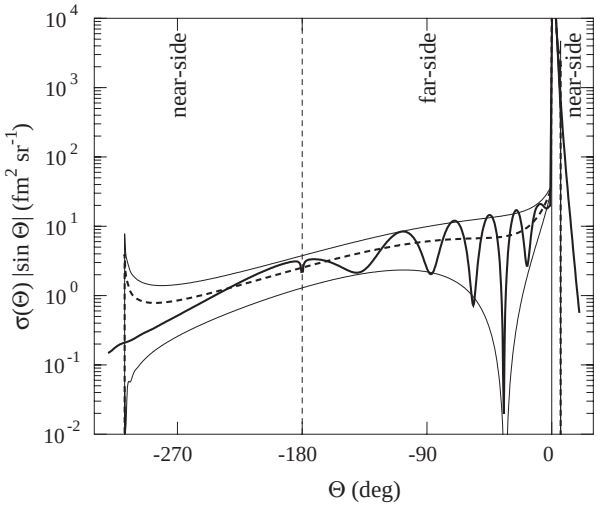

Fig. 5. Unfolded quantum (thick solid line) and classical (thick dashed line) cross-sections, and classical interference limits (thin lines), plotted *versus* the deflection angle.

backward glory singularities. The forward glory is masked by the $\sigma_{\rm R}(\theta)$ higher-order singularity.

In panel (b) the thin solid lines show the classical interference limits of the contributions from all the branches of $\Theta(\lambda)$. In the same panel the thick dashed and solid lines show, respectively, the full classical and the quantum cross-sections. The interference limits were calculated using (13) in the region $\theta_{\rm C} < \theta < \theta_{\rm n}$, where only the two F branches 1 and 4 of $\Theta(\lambda)$ contribute. Four branches contribute for $\theta < \theta_{\rm C}$ (1, 4, 5, and 6) and $\theta > \theta_{\rm n}$ (1, 2, 3, and 4). In these angular regions the interference limits were calculated using (10) and (12).

With the exclusion of a small angular range to the right of $\theta_{\rm C}$, the oscillations appearing in the quantum cross-section are well within the classical interference region. The interference limits cannot, however, be considered the upper and lower envelopes of the quantum $\sigma(\theta)$. The reason for this is clarified in panels (c) and (d), where the N and F components of the quantum and classical cross-sections, respectively, are shown.

Only the branches 1 and 4 contribute to the F classical cross-section in the whole angular range. To the classical N cross-section the branches 5 and 6 contribute for $\theta < \theta_{\rm C}$, while 2 and 3 contribute for $\theta > \theta_{\rm n}$. The reduced number of the branches contributing separately to the classical N and F cross-sections considerably reduces the width of the corresponding interference regions, with respect to that of the full cross-section. Only in the region $\theta_{\rm C} < \theta < \theta_{\rm n}$ the F interference region obviously coincides with the full one.

Thanks to the use of the NF decomposition we can observe that the F interference limits result almost perfect envelopes of the quantum F cross-section. The period of the oscillations of this cross-section decreases with the increase of θ, which corresponds to a decrease of the deflection angle. This is confirmed by the very long period of the oscillation appearing in the backward-angles N cross-section. Owing to this, the oscillations can be interpreted as arising from interference between classical-like contributions whose phase differences tend to decrease while approaching the nuclear-rainbow angular momentum. In the present case, these phase differences are too small to allow us to observe the maximal constructive and destructive interference amongst all the four branches of the $\Theta(\lambda)$ contributing for $\theta > \theta_{\rm n}$.

In the classical N cross-section a dark region is present between $\theta_{\rm C}$ and $\theta_{\rm n}$. From both the shadow boundaries, this dark region appears enlightened by the quantum N cross-section, and the tails of the two shadows overlap without producing relevant interference effects[1].

The N and F cross-section interference patterns are considerably simpler than the full cross-section one. The complicate pattern of the full $\sigma(\theta)$ arises from the coherent superposition of the simpler F and N subamplitudes. It is the folding of the plane of fig. 3, represented in fig. 1, which is responsible for this complicate pattern. The NF decomposition allows one to attempt the unfolding of the quantum cross-section, in analogy to the unfolding of the classical cross-section shown in fig. 2, by considering its dependence on the deflection angle rather than on the scattering angle. In fig. 5 the thick solid curve shows the unfolded quantum cross-section. In order to eliminate the appearance of the classical glory singularities, in this figure, as in fig. 2, the cross-sections multiplied by $|\sin\Theta|$ are plotted. To construct the unfolded quantum cross-section

[1] The interference effects observed in ref. [11] in panel (c) of figs. 2 and 9, and in panels (c) and (d) of fig. 16 (and the corresponding effects in figs. 3, 6, 12, 19, and 20) are artifacts deriving from unphysical contributions present in the usual Fuller's NF decomposition [10], but absent in the improved one [9] here used.

the N cross-section values for $\theta \lesssim 30^\circ$ were attributed to $\Theta = \theta$, and those for $\theta \gtrsim 30^\circ$ to $\Theta = -360^\circ + \theta$. The values of the F cross-section were attributed to $\Theta = -\theta$. The same was obviously done for the classical cross-sections and interference limits.

The unfolded quantum curve thus obtained shows an irregular behavior in a small range around -180°. This is probably due to the fact that the singularities of the quantum N and F cross-sections at 180° are slightly different from the $1/\sin\theta$ singularity predicted by the non-uniform approximation of the Legendre functions. With the exclusion of this small range, one can appreciate the attempt of the N quantum curve ($\Theta < -180^\circ$) to match continuously the F one ($-180^\circ < \Theta < 0^\circ$) at $\Theta = -180^\circ$.

The comparison of $\Theta_{\rm Q}(\lambda)$ with $\Theta(\lambda)$, and the behavior of the F quantum cross-sections with respect to the corresponding interference limits, allows one to recognize the presence, in the quantum quantities, of contributions which are very close to those expected from the asymptotic classical-like limit. The increase of the oscillation period of $\sigma(\Theta)$, with decreasing Θ, well justifies the fact that the interference limits are rather far from representing the envelopes of the "folded" full quantum cross-section, plotted as a function of θ.

3.2 Pure quantum-mechanical analysis

Results similar to those shown in subsect. 3.1 can be obtained without using any classical-mechanics calculation, by simply observing the changes produced in $S(\lambda)$ and in $\sigma(\theta)$ by changing the value attributed to $\hbar$.

In fig. 6 the open dots show the values of $\Theta_{\rm Q}(\lambda)$ calculated at integer λ values using eq. (16) and substituting $\hbar$ in an optical-potential code with $\hbar_f = \hbar/f$, with $f = 0.5, 1.0, 1.5$, and 2.0.

Because the spacing in b of points corresponding to one unit increment of the angular-momentum quantum number l is proportional to $1/f$, the abscissas of the points corresponding to $\Delta l = 1, 2, 4$ for the cases $f = 0.5, 1.0, 2.0$ are trivially the same at appropriate b values. The b value corresponding to $\lambda = 1$ for $f = 0.5$ is the same as that corresponding to $\lambda = 2$ for $f = 1.0$ and to $\lambda = 4$ for $f = 2.0$, and so on. In fig. 6 the open dots corresponding to these values of f result perfectly concentric at the common b values, with the exclusion of a small range around $b \simeq 5.5$. This provides a striking confirmation of the classical scale invariance properties of $\Theta_{\rm Q}(\lambda)$ for almost all the values of the angular-momentum quantum number. The thick solid curve, representing $\Theta(\lambda)$, shows that also in the above small range, and in the more unfavorable case ($f = 0.5$, $\hbar$ two times larger), the agreement between $\Theta_{\rm Q}(\lambda)$ and $\Theta(\lambda)$ is rather good. This agreement becomes practically perfect for the most favorable case ($f = 2.0$, $\hbar$ two times smaller).

The tendency of all the $\Theta_{\rm Q}(\lambda)$ points (plotted against b for different $\hbar$ values) to lie on the same curve is a clear sign of the fact that the properties of $S(\lambda)$ (with the true $\hbar$ value) are very close to those predicted by the asymptotic classical-like limit (6). This can be tested using only quantities calculated by a conventional optical-potential code, without the necessity of calculating the classical deflection function.

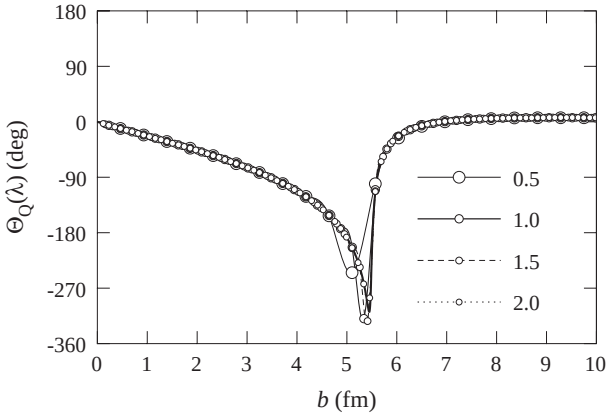

Fig. 6. Quantum deflection functions (open dots) calculated using the four $\hbar$ reduction factors given in the figure. The thin curves interpolate the dots, the thick one shows the classical deflection function.

Panels (a), (b) and (c) of fig. 7 show, respectively, the full, N and F cross-sections calculated with the above values of the reducing factor f. In these figures the thick dashed and thin solid lines show the classical cross-sections and their interference limits, respectively. These lines were drawn only to recall the behavior of these quantities. As for the deflection function, their knowledge is not necessary to recognize the presence of classical-like contributions.

In the insets, showing a reduction of each panel, the true cross-sections are plotted together with eleven cross-sections calculated with values of f ranging from 3.0 to 4.0 with a step of 0.1.

By looking at fig. 7 (a) one observes a rather complicate behavior of the full cross-sections corresponding to the four values of f from 0.5 to 2.0. This makes it difficult to imagine that the oscillations tend to be confined within a well-defined region. This tendency begins to appear in the inset, where a rather well-defined upper envelope can be observed, and also indications of a lower envelope are present. The minor definiteness of the lower envelope is explained by the fact that, with the scale used, the minima are much narrow than the maxima. Using a fixed grid to tabulate the cross-sections it is more probable to miss a minimum rather than a maximum.

For $\theta_{\rm C} < \theta < \theta_{\rm n}$, the full cross-sections calculated with the four values of f are in disagreement with the interference limits, particularly in the region to the right of $\theta_{\rm C}$. The disagreement decreases rapidly with increasing f.

The reason of this behavior is understood by considering fig. 7 (b), where the N cross-sections are plotted. In the classical shadow region, by increasing f, the cross-sections decrease very rapidly moving to the right of $\theta_{\rm C}$, while they decrease slowly moving to the left of $\theta_{\rm n}$. In the inset one can observe that even for f values ranging from 3.0 to 4.0 the decrease of the N cross-section is slow, moving from

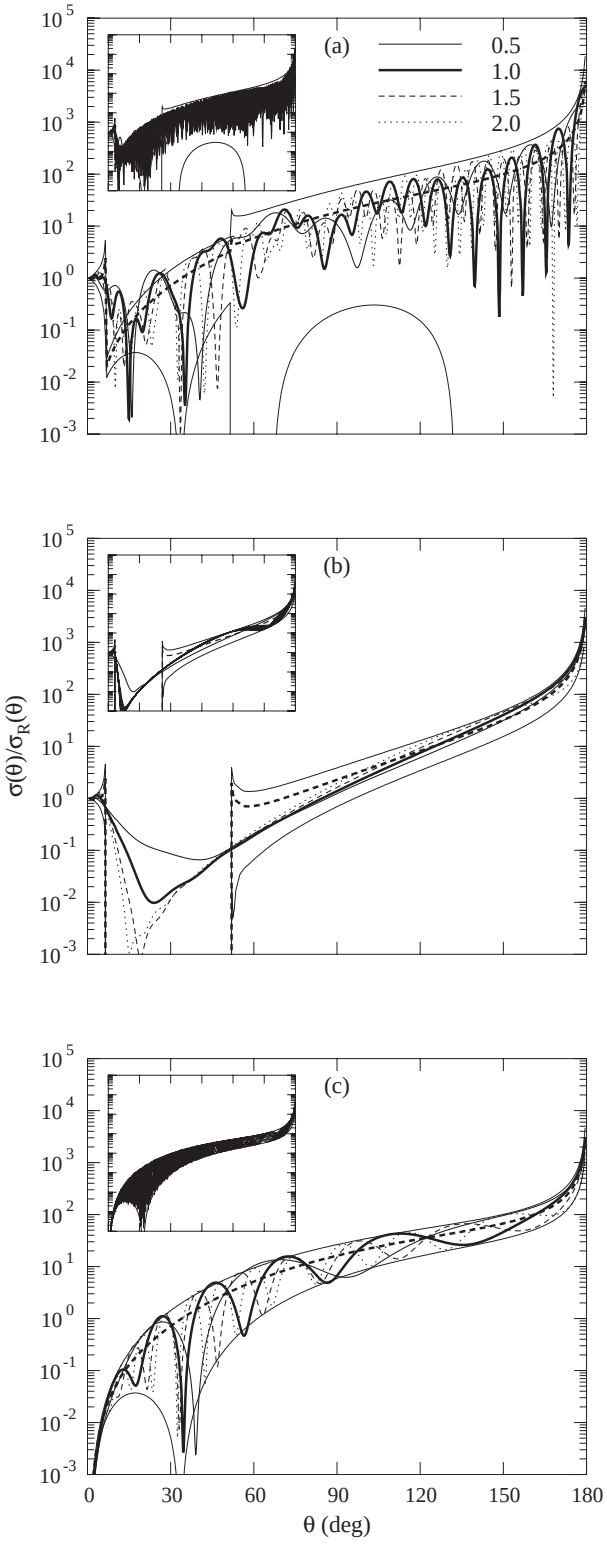

Fig. 7. Full (a), N (b) and F (c) quantum cross-sections, for the four $\hbar$ reduction factors given in panel (a), together with the classical cross-section (thick dashed) and interference limits (thin solid). The quantum cross-sections and the classical quantities are plotted in the insets together with quantum cross-sections calculated with $\hbar$ reduction factors from 3 to 4.

the right towards the classical shadow region. The eleven cross-sections only begin to fill gradually the interference region. The phase difference between the subamplitudes, contributing to this part of the N cross-section, depend weakly on the angle and only a few oscillations appear in the cross-section at the maximum value of f considered.

In the asymptotic estimate of the scattering amplitude using the uniform method around a rainbow angle, the rapidity of the decrease of the cross-section, in the classical shadow region, depends on the second derivative of the deflection function at the rainbow angular momentum. The curvature of the deflection function is much higher at the nuclear than at the Coulomb rainbow, and this explains why the two slopes are so different.

The full and the N cross-sections do not clearly exhibit properties which are invariant with respect to the value attributed to $\hbar$. This is not the case for the F cross-sections shown fig. 7 (c). The existence of common upper and lower envelopes for these cross-sections is rather well indicated already by the f values ranging from 0.5 to 2.0, and is clearly proved by the f values from 3.0 to 4.0 given in the inset of the figure. Apart from a very small distortion of at least one of the two interfering subamplitudes this figure provides a strong indication of the dominance of classical-like contributions already from the value $f = 0.5$ ($\hbar$ two times larger).

4 Complex optical-potential cross-section: $E_{lab} = 132$ MeV

The first complex optical potential considered is one of the potentials whose cross-section fits the experimental data at $E_{\rm lab} = 132$ MeV [4]. The imaginary part of the potential has a conventional Woods-Saxon form factor with parameters $W_0 = 13.86$ MeV, $R_w = 5.6894$ fm, and $d_w = 0.656$ fm. The parameters of the real part are those of the real optical potential previously considered.

This case was chosen because a recent semiclassical analysis [14], using the Brink and Takigawa [15] approximation, has shown that the oscillations appearing in the F cross-section can be explained as arising from the interference between the F contributions from the first two terms, named in the following *barrier* and *internal*, of the multireflection expansion of the semiclassical scattering amplitude. A similar result has also been obtained [16,17] (with an approximate calculation [18] of the barrier and internal amplitudes) for the same and for several other optical potentials used to describe the elastic scattering of light heavy-ions.

Because the F contribution to the barrier term is responsible for the appearance of the Fraunhofer-like pattern in the barrier cross-section, one is naturally induced to think that this contribution should be considered of diffractive nature, *i.e.* of quantum origin. It seems therefore interesting to check this interpretation with the simple recipe here proposed. By decreasing the value of $\hbar$, one should also observe how this contribution changes, becoming a classical-like one.

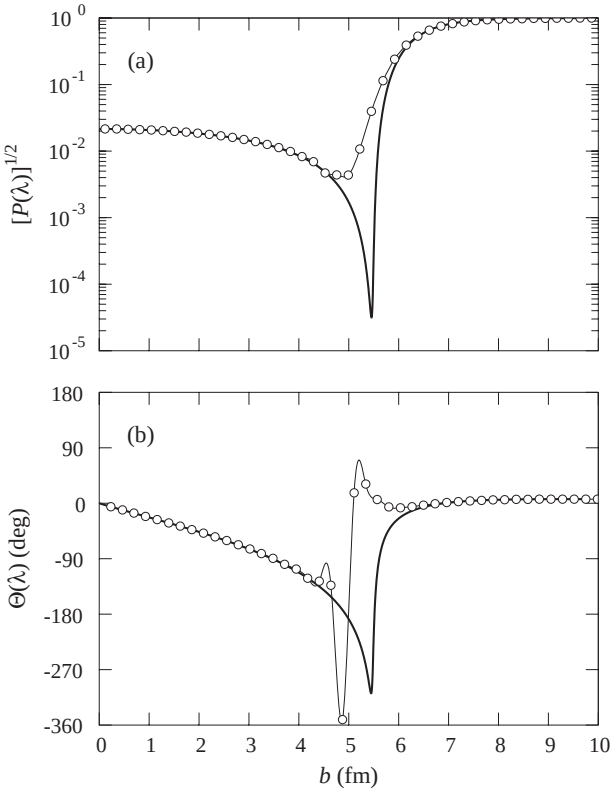

Fig. 8. The thick curves show the classical deflection function (b) and the square root of the survival probability (a). The open dots represent the values of the quantum deflection function and of the modulus of the scattering function. The thin lines interpolate the dots.

4.1 Comparison with classical quantities

According to the above classical interpretation of the imaginary part of the potential, the presence of this term introduces a probability $P(\lambda)$ of survival in the elastic channel, but does not modify the classical deflection function $\Theta(\lambda)$. Owing to this, the same labels of fig. 1 can be used to identify the contributions from the different branches of $\Theta(\lambda)$.

In panels (a) and (b) of fig. 8 the thick lines show, respectively, the square root of $P(\lambda)$ and $\Theta(\lambda)$ as functions of the impact parameter b. In the same figure the dots represent the values of $|S(\lambda)|$ and of $\Theta_{\rm Q}(\lambda)$ and the thin lines are cubic spline interpolations of the dots. The figure shows that the quantum and classical corresponding quantities are in good agreement, apart from a neighborhood around $b \simeq 5.5$ fm of half-width of about 1 fm. The impact parameter value $b_{\rm n}$ of the nuclear rainbow is in this region, and its position is very close to the position of the deep minimum of $P(\lambda)$. The behavior of $|S(\lambda)|$ in this region is considerably different from that of the square root of $P(\lambda)$. This suggests the dominance of a scattering mechanism different from a classical-like one for the angular momenta corresponding to this range of impact parameters.

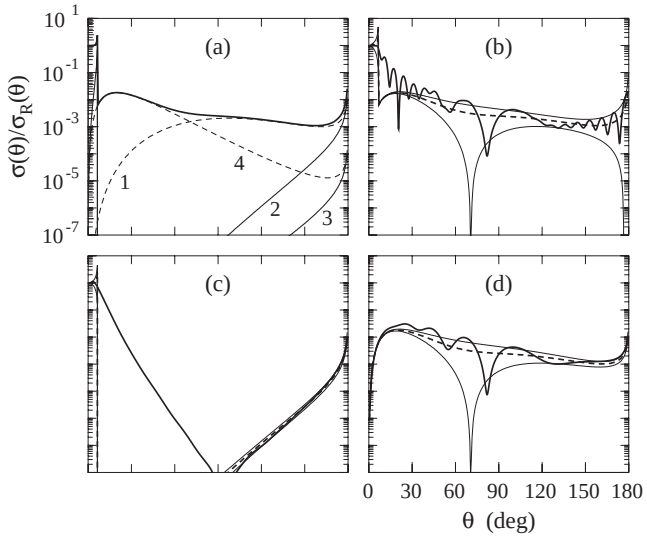

Fig. 9. The same as fig. 4 for the complex optical potential at $E_{\rm lab} = 132$ MeV.

In the different panels of fig. 9 the same quantities given in the corresponding panels of fig. 4 (real potential) are shown for the complex potential. At angles larger than $\theta_{\rm C}$ the contributions from all the branches of the deflection function are strongly reduced by the absorption. Each point of the old curves is lowered by the corresponding value of $P(\lambda)$. Furthermore, the deep minimum of $P(\lambda)$, around $b_{\rm n}$, produces a dramatic reduction of the contribution from the N trajectories with $b \simeq b_{\rm n}$. Only part of the N contributions from the branches 2 and 3 of $\Theta(\lambda)$ can be observed within the range of the vertical axis of fig. 9. At backward angles these curves are close to the dashed lines representing the F contributions from the branches 1 and 4 of $\Theta(\lambda)$, but they drop very rapidly with decreasing angle going out from the plotted area. The very small values of these contributions at angles just above $\theta_{\rm n}$ prevent the observation of effects in the classical cross-section deriving from the nuclear-rainbow singularity.

The rapid decrease of these contributions, together with the modifications of the slopes of the contributions from the F trajectories, considerably shrinks the width of the interference region. The borders of this region are shown by the thin lines in panel (b) of fig. 9. In the same panel, the thick curve shows the quantum cross-section. This curve, in the forward hemisphere, substantially violates the boundaries fixed by the interference limits.

Panel (c) shows that the violation of the interference limits is mainly due to a violation of the corresponding limits by the N component of the full cross-section. At angles to the right of $\theta_{\rm C}$ the quantum curve decreases almost exponentially, at the rate of about one order of magnitude per 10°, filling the classical shadow region and crossing the backward interference region at about 90°. In the backward hemisphere, decreasing θ below 180°, the quantum N curve closely follows the classical cross-section of the branch 2 of the deflection function. This behavior is qualitatively similar to that observed in the N cross-section of

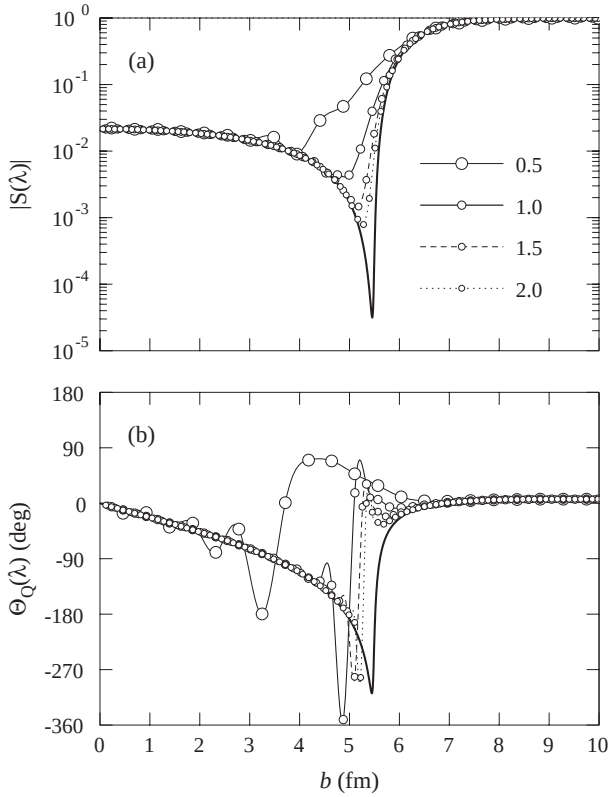

Fig. 10. The open dots show the moduli of the scattering functions (a) and the quantum deflection functions (b) calculated using the four $\hbar$ reduction factors given in the figure. The thick curves show the corresponding classical quantities and the thin curves interpolate the dots.

the real potential. The only difference is represented by the fact that now the curves at the right of $\theta_{\rm n}$ are downward shifted and decrease more rapidly by decreasing the angle. This allows one to observe in a wider angular range the almost exponential decrease to the right of $\theta_{\rm C}$.

The behavior of the quantum F cross-sections (panel (d)) show that a relevant contribution to the violation of the classical interference limits comes also from at least one of the subamplitudes responsible for the oscillations of this cross-section. This supports the results obtained with the semiclassical analysis [14], suggesting that one of these subamplitudes cannot be considered a classical-like one.

4.2 Pure quantum analysis

Panels (a) and (b) of fig. 10 show, respectively, $|S(\lambda)|$ and $\Theta_{\rm Q}(\lambda)$ calculated with the four values of f from 0.5 to 2.0, and correspondingly scaling the imaginary part of the potential. By increasing f all the points tend to lie on the same curve in increasing ranges of b. Comparing the behavior of the points representing $\Theta_{\rm Q}(\lambda)$ with the corresponding ones for the real potential one observes that the imaginary part of the potential delays the approach of the classical-like limit. The addition of an imaginary part increases the non-homogeneity of the medium in which the particles propagate and favors the survival of wave effects.

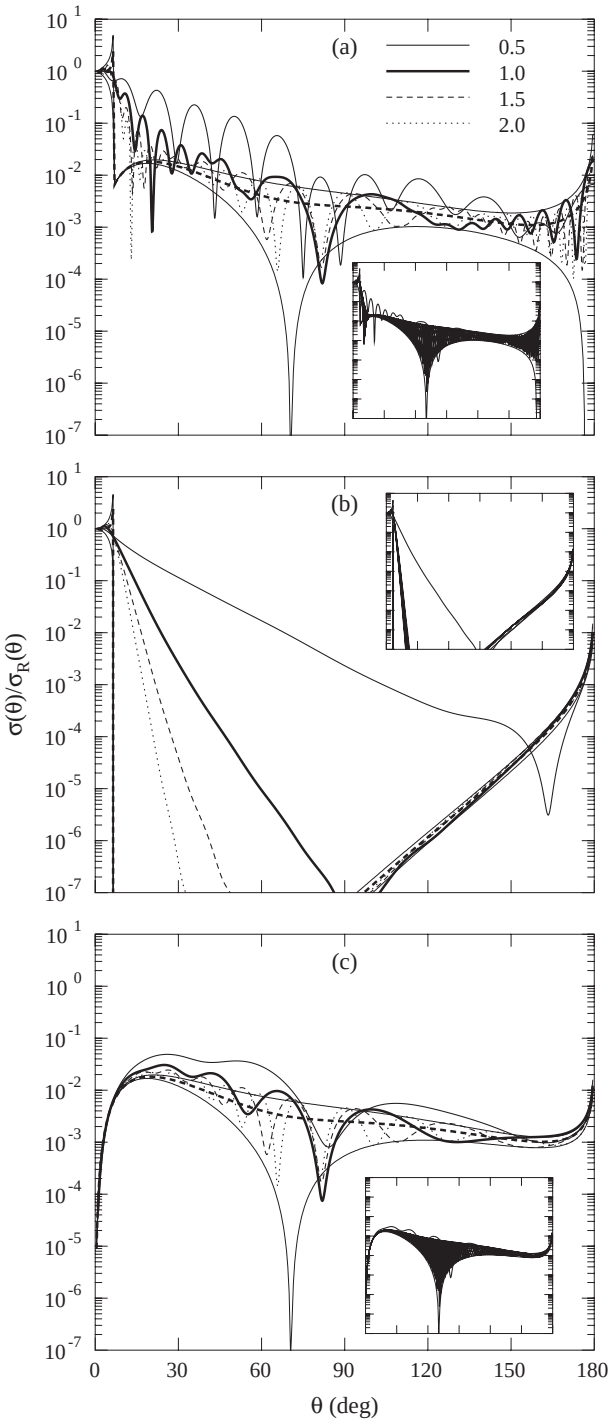

Fig. 11. The same as fig. 7 for the complex optical potential at $E_{\rm lab} = 132$ MeV.

It is interesting to observe that, for $f = 0.5$ and b larger then about 4 fm, $\Theta_{\rm Q}(\lambda)$ has characteristics typical of a repulsive interaction. These are similar to those of the deflection function of the barrier term of the Brink and Takigawa approximation, which accounts for the con-

tribution from the reflection phenomenon of the incoming waves in the region of rapid variation of the interaction.

The variations with f of the full, N and F cross-sections are shown in panels (a), (b) and (c) of fig. 11, respectively. In these figures the full and F cross-section curves corresponding to values of f from 0.5 to 2.0 are rather far from having common envelopes. In the backward hemisphere the N cross-section depends very few on $\hbar$ for $f \geq 1$, while the common envelopes begin to appear in the full and F cross-sections with $f = 1.5$ and 2.0. The existence of a well-defined interference region is clearly shown by the calculations with values of f from 3.0 to 4.0, given in insets.

Thanks to the rapid decrease of the N cross-section, by decreasing the angle below 180°, the boundaries of the interference region are far better defined for the complex potential full cross-section than for the real potential one. The addition of the imaginary part to the optical potential has strongly increased the slope of the backward N cross-section and has considerably reduced, or perhaps eliminated, the long period oscillations appearing in the inset of fig. 7 (b). Both these facts contribute to a better definition of the interference region for the full cross-section.

The interference region, obtained using a pure quantum calculation, is just the one previously calculated using the classical mechanics. This confirms that the analysis of the nature of the different contributions to the cross-section can be done in absence of any classical-mechanics calculation.

The presence of at least one classical-like contribution in the F cross-section is proved by the behavior of this cross-section at backward angles, and by its continuation, passing through the glory singularity, in the N cross-section at backward angle. The violation, at forward angles, of the interference limits suggests that the other subamplitude, responsible for the oscillations of the F cross-section, cannot be considered a classical-like one.

5 Complex optical-potential cross-section: $E_{lab} = 200$ MeV

The second complex optical potential considered is one of the potentials whose cross-section fits the experimental data at $E_{\rm lab} = 200$ MeV [4]. This potential also has conventional Woods-Saxon form factors with parameters $V_0 = 216.3$ MeV, $R_v = 3.2847$ fm, $d_v = 0.927$ fm, for the real part, and $W_0 = 17.83$ MeV, $R_w = 5.8625$ fm, and $d_w = 0.541$ fm for the imaginary part.

This case was considered because an analysis similar to that of ref. [14] shows that the semiclassical Brink and Takigawa method fails to reproduce quantitatively the optical cross-section in the whole angular range [11]. Owing to this, the semiclassical method cannot be used to try to attribute a physical meaning to the different terms contributing to the cross-section. The hope is that the present recipe provides useful indications on the nature of the subamplitudes contributing to the cross-section of this potential.

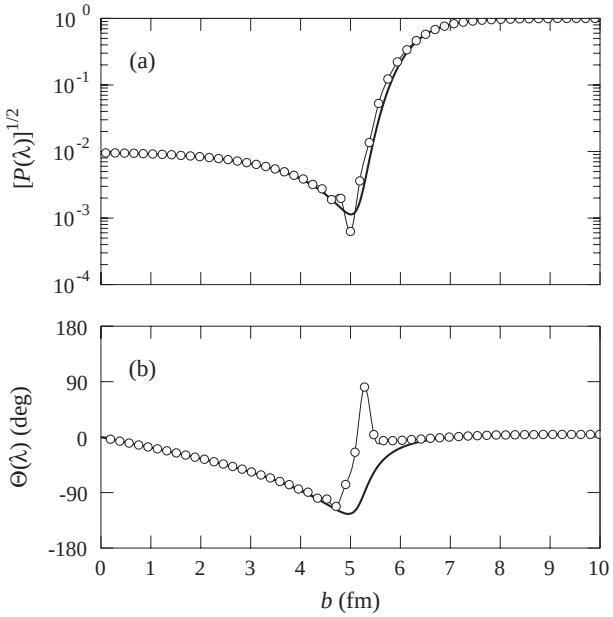

Fig. 12. The same as fig. 8 for the complex optical potential at $E_{\rm lab} = 200$ MeV.

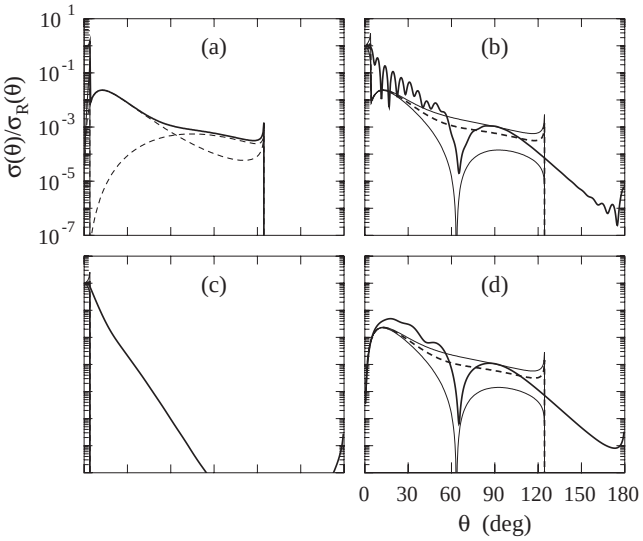

Fig. 13. The same as fig. 4 for the complex optical potential at $E_{\rm lab} = 200$ MeV.

5.1 Comparison with classical quantities

In fig. 12 the classical $\Theta(\lambda)$ and the square root of $P(\lambda)$ are shown together with the corresponding quantum quantities. With respect to the 132 MeV case, the minimum of the deflection function corresponding to the nuclear rainbow has moved to a deflection angle $\Theta_{\rm n} \simeq -125°$. Because the nuclear-rainbow singularity slits [19] toward a deflection angle larger than $-180°$, the backward glory singularities are suppressed, and only four branches of the deflection function contribute to the cross-section. The panels of fig. 13 show that, in this case, the regions to the right of the Coulomb rainbow $\theta_{\rm C}$ (for the N cross-section) and

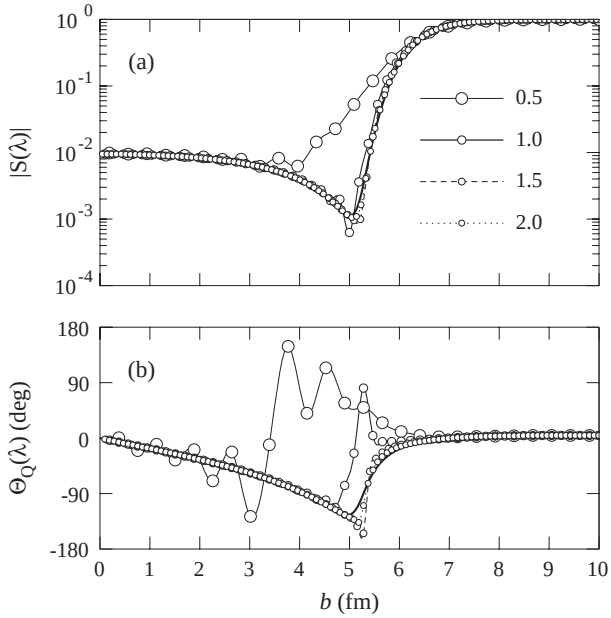

Fig. 14. The same as fig. 10 for the complex optical potential at $E_{\rm lab} = 200$ MeV.

to the right of the nuclear rainbow $\theta_{\rm n}$ (for the F and the full cross-sections) are classical shadow regions.

The quantities $\Theta_{\rm Q}(\lambda)$ and $|S(\lambda)|$ are in substantial agreement with the corresponding classical ones in b ranges wider than for the 132 MeV case. However, the violations of the interference limits of the quantum full and F cross-sections, shown in panels (b) and (d) of fig. 13, are not smaller than in the lower energy case. For angles smaller than about 60° the F quantum cross-section is largely outside of the classical interference region. This suggests that also for this potential, as for the 132 MeV case, these oscillations cannot be interpreted as arising from the interference between two classical-like contributions.

5.2 Pure quantum analysis

For the 200 MeV potential, figs. 14 and 15 correspond to figs. 10 and 11, for the 132 MeV case. By comparing fig. 14 with fig. 10 one observes that, by decreasing $\hbar$, the properties of $S(\lambda)$ approach the classical-like limit faster in the higher-energy case. This is true also for the properties of the cross-sections, and depends on the fact that for higher energy the wavelength is smaller. In particular, by looking at fig. 15 (a) and (c) one observes that the quantum curves begin to have as upper and lower envelopes the interference limits, for scattering angles around 60°, already with a $\hbar$ reducing factor of 1.5. From this value upward the interference pattern, below the classical nuclear-rainbow angle, can be considered as arising from interference between classical-like contributions.

In the insets of fig. 15 (a) and (c) one again observes that the quantum calculations, with f values ranging from 3.0 to 4.0, very well define the classical interference region,

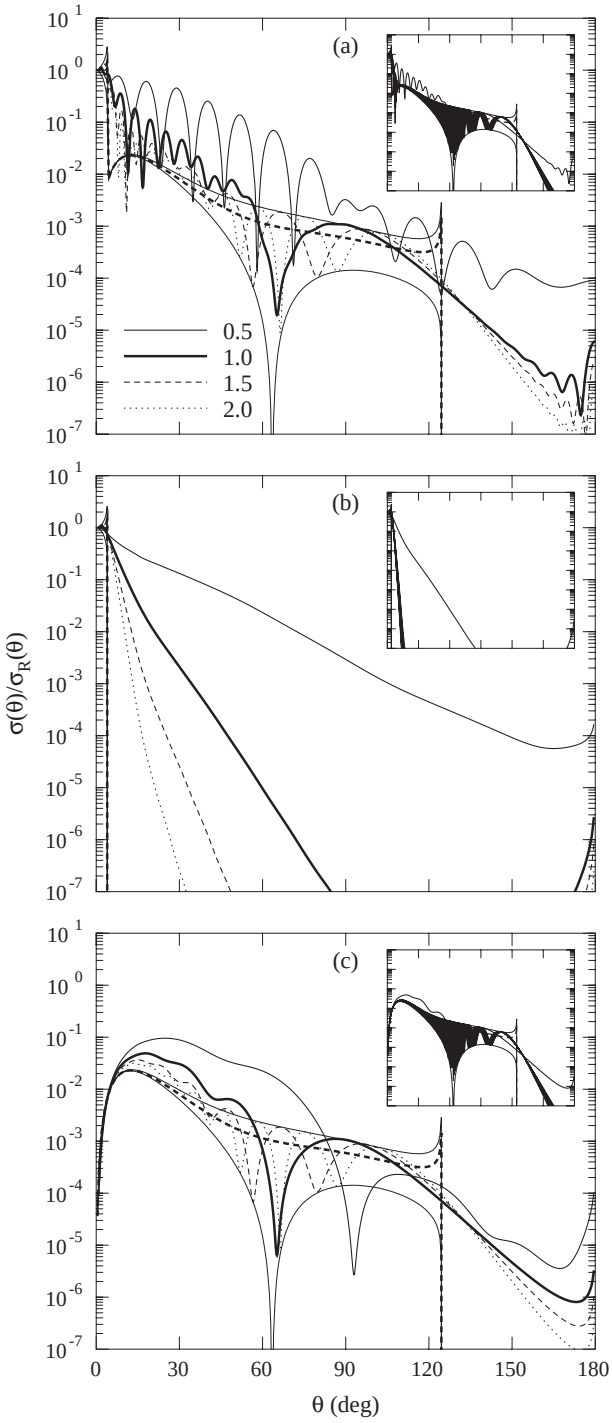

Fig. 15. The same as fig. 7 for the complex optical potential at $E_{\rm lab} = 200$ MeV.

apart from the standard problems connected with the quantum behavior around the classical nuclear-rainbow angle. Also in this case, the good definition of the interference region allows one the test the classical-like origin of the different subamplitudes contributing to the quantum cross-section by using only the calculations of a standard optical-potential code.

In the forward hemisphere, the values of the true F cross-section largely violates the interference limits. Figure 15 (b) shows that, as in the previous case, the behavior of the N cross-section in the classical shadow region is largely responsible for the violation of the interference limits of the full cross-section. In the inset of the same figure one can observe that, for f values from 3.0 to 4.0 and for $\theta > \theta_C$, only the rapidly decreasing exponential contribution appears in a very restricted angular range above θ_C.

6 Conclusions

The simple recipe of shrinking $\hbar$, in a conventional optical-potential calculation, provides useful information on the nature of the different subamplitudes contributing to the cross-section.

By decreasing $\hbar$ the different characteristics of the cross-section smoothly change, with different rapidity. In the major part of the angular interval, below some $\hbar$ value, no further changes are observed in the cross-sections with decreasing $\hbar$, apart from the sliding of the interference pattern within well-defined regions, with an increasing number of oscillations. These are the characteristics connected with the realization of the transition from the dynamical regime governed by quantum mechanics to that well approximated by its asymptotic classical-like limit.

The recipe can be easily implemented in any optical-potential code, providing a practical tool for a rapid check of the classical-like properties of the cross-section of a given potential.

The possibility of producing optical-potential cross-sections, attributing different values to $\hbar$, can also be used as a laboratory, providing useful cross-sections for testing the effectiveness of the semiclassical techniques currently used for investigating the subtle transition between the quantum and the classical-like regimes.

References

1. Dao T. Khoa, W. von Oertzen, H.G. Bohlen, F. Nuoffer, Nucl. Phys. A **672**, 387 (2000).
2. M.P. Nicoli, F. Haas, R.M. Freeman, N. Aissaoui, C. Beck, A. Elanique, R. Nouicer, S. Szilner, Z. Basrak, A. Morsad, M.E. Brandan, G.R. Satchler, Phys. Rev. C **60**, 064608 (1999).
3. M.P. Nicoli, F. Haas, S. Szilner, Z. Basrak, A. Morsad, G.R. Satchler, M.E. Brandan, Phys. Rev. C **61**, 034609 (2000).
4. A.A. Ogloblin, Yu. A. Glukhov, W.H. Trzaska, A.S. Dem'yanova, S.A. Goncharov, R. Julin, S.V. Klebnikov, M. Mutterer, M.V. Rozhkov, V.P. Rudakov, G.P. Tiorin, Dao T. Khoa, G.R. Satchler, Phys. Rev. C **62**, 044601 (2000).
5. S. Szilner, M.P. Nicoli, Z. Basrak, R.M. Freeman, F. Haas, A. Morsad, M.E. Brandan, G.R. Satchler, Phys. Rev. C **64**, 064614 (2001).
6. M.E. Brandan, A. Menchaca-Rocha, L. Trache, H.L. Clark, A. Azhari, C.A. Gagliardi, Y.-W. Lui, R.E. Tribble, R.L. Varner, J.R. Beene, G.R. Satchler, Nucl. Phys. A **688**, 659 (2001).
7. D.M. Brink, *Semi-Classical Methods for Nucleus-Nucleus Scattering* (Cambridge University Press, Cambridge, 1985).
8. K.W. Ford, J.A. Wheeler, Ann. Phys. (N.Y.) **7**, 259 (1959).
9. R. Anni, J.N.L. Connor, C. Noli, Phys. Rev. C **66**, 044610 (2002), nucl-th/0111060.
10. R.C. Fuller, Phys. Rev. C **12**, 1561 (1975).
11. R. Anni, nucl-th/0102030.
12. R. Broglia, S. Landowne, R.A. Malfliet, V. Rostokin, Aa. Winther, Phys. Rep., Phys. Lett. C **11**, 1 (1974).
13. R. Anni, Phys. Rev. C **63**, 067601 (2001).
14. R. Anni, Phys. Rev. C **63**, 031601 (2001).
15. D. Brink, N. Takigawa, Nucl. Phys. A **279**, 159 (1977).
16. F. Michel, F. Brau, G. Reidemeister, S. Ohkubo, Phys. Rev. Lett. **85**, 1823 (2000) .
17. F. Michel, G. Reidemeister, S. Ohkubo, Phys. Rev. C **63**, 034620 (2001).
18. J. Albiński, F. Michel, Phys. Rev. C **25**, 213 (1982).
19. K.M. McVoy, Nucl. Phys. A **455**, 141 (1986).